Physically-based Deformation of High-Resolution 3D Lung Models for Augmented Reality based Medical Visualization

Anand P Santhanam[1],Cali M Fidopiastis[2],Felix G Hamza-Lup,[1]
Jannick P Rolland[123], and Celina Imielinska[4]

[1]School of Computer Science, University of Central Florida
[2]Institute of Simulation and Training, University of Central Florida
[3]College of Optics and Photonics: CREOL & FPCE, University of Central Florida
4000 Central Florida Blvd Orlando FL 32816 USA
{anand,cali,felix,jannick}@odalab.ucf.edu,
[4]Department of Bio-informatics, Columbia University
New York, USA
ci42@columbia.edu

Abstract. Visualization tools using Augmented Reality Environments are effective in applications related to medical training, prognosis and expert interaction. Such medical visualization tools can also provide key visual insights on the physiology of deformable anatomical organs (e.g. lungs). In this paper we propose a deformation method that facilitates physically-based elastostatic deformations of 3D high-resolution polygonal models. The implementation of the deformation method as a pre-computation approach is shown for a 3D high-resolution lung model. The deformation is represented as an integration of the applied force and the local elastic property assigned to the 3D lung model. The proposed deformation method shows faster convergence to equilibrium as compared to other physically-based simulation methods. The proposed method also accounts for the anisotropic tissue elastic properties. The transfer functions are formulated in such a way that they overcome stiffness effects during deformations.

1 Introduction

Augmented Reality (AR) environments allow the development of promising tools in medical applications.[1] One such medical application is the 3D lung visualization.[2] An essential requirement for visualizing 3D lung dynamics is to predict the 3D lung model shapes by deforming a given 3D lung model with time. In order to accurately deform a 3D lung model, physically-based deformation (computing displacement) methods are required.[3] Physically-based methods for 3D deformations can be found in

areas ranging from animations to surgical simulations. High-resolution models are 3D models with a large number of elements (e.g. nodes, triangles) which are created using advanced imaging technologies.[4] These models provide extensive scope to meticulously associate tissue properties with its nodes. The size of these models increases the computational complexity of the physically-based deformation and graphical rendering thereby affecting the real-time requirements of the application.

The main aim of the proposed method is to obtain a real-time physically-based deformation of high-resolution 3D anatomical models, as well as its visualization in an AR environment [5] as shown in Fig 1. We consider the high-resolution 3D lung surface models obtained from the visible human dataset [4], to be deformed using a physically-based deformation method. The main contribution of this paper is (a) to propose an pre-computed elastostatic deformation algorithm with a low run-time complexity in order to deform high-resolution lung models in an AR environment (b) to compare the proposed method with other physically-based deformation algorithms for accuracy and computational issues.

The paper is structured as follows. Section 2 summarizes the related work on physically-based deformation algorithms, tissue deformation methods and lung deformation methods**.** Section 3 summarizes the physiology of lung that applies to its deformation**.** Section 4 discusses the proposed deformation method. Section 5 compares the proposed method with physical simulation methods. Section 6 concludes the paper.

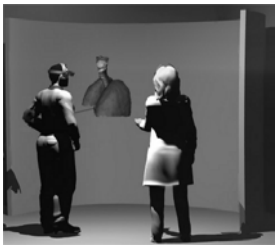

(Fig.1a)

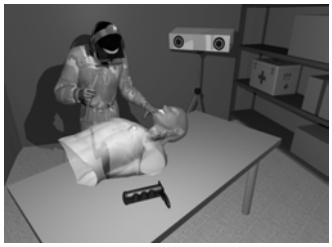

(Fig.1b)

Fig. 1a-b. Visualization of non-deforming lungs in **(a)** the ARC display and **(b)** when registered with a Human Patient Simulator (Courtesy: Stephen Johnson)

2 Prior work

In this section we present related work on physically-based deformation methods followed by a discussion on tissue and lung deformation methods.

2.1 Physically-based Deformations

Initial models for physically-based deformations were pioneered by [3, 6, 7]. While Platt used mass-spring models for creating animated facial expressions, Terzopolous [3] used Finite Difference Methods to create simple animations. These methods represent the mechanics of deformation as a second-order differential equation of the position change for a vertex on the 3D model. The Finite Difference Method was further modified to simulate plasticity and fractures by [6]. These formulations were computationally expensive for high-resolution models. Some of the improvements that lowered the computational complexity were focused on either decimating the 3D model or simplifying the equation complexity. The first approach [8] used graph simplification algorithms while the second approach [9] used matrix simplification methods. An integration of both approaches was done using multi-resolution wavelets [10].

Of particular importance was the linearization of deformations. Iterative solutions for the first-order differential equation of deformation were as described in [11]. Iterative methods were further investigated in [12]. Once the deformation was computed for a given force, it was linearly scaled for any force that deforms the object. Interactive deformations were obtained using pre-computed tensors [13]. The non-linearity in deformations occurs only for large and torsional deformations. The methods proposed for compensation [14] did not allow pre-computation.

2.2 Physically-based Tissue Deformations

The methods for representing the change in shape of a tissue were discussed based on its bio-mechanical properties.[15] These methods further provide a scope for the use of elastostatic methods [16] for modeling tissue deformations. An analysis of soft-tissue modeling using the linearized elastostatic reversible deformation approach was introduced by Delingette.[17] To deform models that represent tissue samples and organs, Finite Element Methods (FEM) were also used and the computations were further optimized using condensation techniques.[9] The inability of linearized deformation approach to model rotational tissue deformations was addressed by Ayache. A non-linear tensor model based on St. Venant-Kirchoff model was further discussed.[18] Linear Element Methods [19] based on tensor deformations were introduced in order to model interactive tissue deformations. This method was further modified to include torsional deformations and was referred to as Radial Element Methods. [20] The scalability and run-time complexity of these methods for deforming high-resolution models need to be further addressed.

An approach of particular importance which is based on weak FEM [11] with hierarchical levels of detail for soft tissue simulation was presented by [21]. In this method, a Green's function is used for representing the strain tensors. The stress (force per unit area) tensor is represented as a convolution equation of integration time for visco-elastic materials. The transfer functions were further computed using an iterative approach. The anisotropic elasticity of the tissue is taken into account for every element

by using a negative exponential function of the Lame's constants[22] of its neighboring elements.

2.3 Lung Deformations

Lung deformations have been studied for the verification of medical imaging equipments and for medical training purposes. The initial observations on lung by Mead based on analysis of moment-of-inertia concluded the deformations to be non-vibrational. [23] The initial methods to model the lung deformation were based on physiology and clinical measurements.[24] The deformation of the lung model as a linearized model was proposed by Promayon. [25] An FEM based deformation was proposed by Kaye in order to model pneumothorax related conditions. The method had an analogy for lung deformations to an electrical circuit. [26] A non-physically-based method to lung deformations was proposed using NURBS surfaces based on imaging data from CT scans of actual patients. [27] The usage of a high-resolution model for lung deformations was not addressed in these efforts.

3 Lung Physiology and its Shape

The deformation of the lungs during inhalation is caused by the following mechanism. During inhalation, the intercostals muscles around the rib-cage move forward, and the diaphragm, the muscle beneath the lungs, moves downward simultaneously. These movements cause the pressure changes in the pleural cavity surrounding the lungs and the alveoli thus allowing the air from the atmosphere to flow inside the lungs.

The non-uniformity in change of shape of lungs for an increase in volume can be further explained as follows. In the normal individual behavior in the upright position, there is a natural intra-pleural pressure gradient from the upper lung region to the lower region. The negative intra-pleural pressure at the lung's apex is normally greater than at the base. This gradient is gravity dependent and is thought to be caused by the normal weight distribution of the lungs. Because of the greater negative pressure in the upper lung regions, the alveoli in those regions are pre-expanded more than the alveoli in the lower lung regions. Therefore the compliance of the alveoli in the upper lung regions is normally less than the compliance of the alveoli in the lower lung region in a normal person in the upright position, which leads to the non-uniformity in change in shape. The deformation of lungs has minimal torsion since the intra-pleural fluid fills the intermediate space [27]. Also the viscous nature of air does not cause any torsional effects since the force due to pressure difference follows Bernoulli's formulations.[28]

The lung model surface discretization into a mesh affects the shape of the lungs. For any change in the mesh tessellation, the variation in the deformation depends upon the number of nodes used on that given surface, which is as shown in Fig 2. In this case, the

irregular meshes are created by removing links from a regular mesh, with a probability of 0.1. It can be seen that the higher the number of nodes on a given surface, the lesser the variation in deformation for any variation in tessellation.

4 Proposed Method

In this section we first discuss the overview of our approach. It is followed by the proposed model discretization and displacement computation methods.

4.1 Overview of our approach

The linearized force balance equation for elastic objects is simplified as given by [9]:

$$KD = f, \quad \textbf{(4.1)}$$

where K is the differential stiffness matrix, D is the displacement vector, and f is the applied force expressed as a vector. It can be seen that equation (4.1) is a discrete form representation considering a set of points in a given 3D model. In order to compute the displacement vector for each of those points, a converging iterative method can be used. The converging iterative method computes the value of the stiffness matrix in a sequence of iterative steps until the stiffness matrix reaches zero or until the cumulative summation of the stiffness matrix during the iterations becomes a constant. The second approach has been successfully used by [21] along with a negative exponential function. In the proposed method we introduce a modification on the Hauth's iterative solution, by replacing the exponential function with a transfer function to model variations in mesh connectivity of the 3D model representation and anisotropic elasticity.

4.2 3D Model Representation

We consider a 3D polygonal model. Each node in the polygonal model has an associated attribute which represents a value equivalent to the local shear modulus.[22] For each link of the polygonal model, we add a node called a spring node. A schematic representation of the proposed 3D model is as shown in Fig 3. The corresponding representation using a mass-spring model is also shown. In the proposed approach on every mass node a force is applied. The force applied on a spring node is initially set to 0. A schematic representation of force application is as shown in Fig 4.

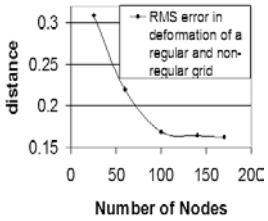

(Fig. 2)

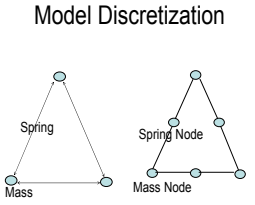

(Fig. 3)

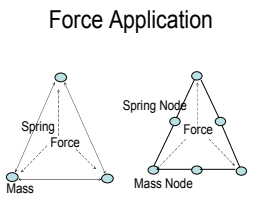

(Fig. 4)

Fig.2. A graph showing the difference in deformation between a regular and an irregular mesh connectivity. **Fig.3.** A schematic representation of a discrete 3D model using the proposed approach and the corresponding representation using a mass-spring model.[7] **Fig.4.** A schematic representation of force application in the proposed approach as well as in the mass-spring model.

4.3 Displacement Computation

The displacement *D[i]* of the ith node, with a mass *M[i]* is computed using an explicit Euler's integration approach [29] with the acceleration during time interval *t* computed as follows

$$\frac{d^2 D[i]}{dt^2} = \frac{F[i]}{M[i]} \ , \qquad \textbf{(4.2)}$$

where *F[i]* is an elastostatic force and is computed for every node based on the force applied on it directly and by the neighboring nodes. We start by initializing a shear modulus value for each node. The spring nodes are assigned values based on their shear modulus while the mass nodes are assigned values based on the inverse of their shear modulus. The transfer function from one node to another is computed based on the proposed equations. An iterative representation of the elastostatic force on each node can be given as

$$F[i] = f[i] * T[i \to i] + \sum_{\substack{\text{clique of i} \\ j=0,\, j \neq i}} F[j] T[j \to i] \ , \qquad \textbf{(4.3)}$$

where *f[i]* is the initial applied force on a node *i* and *T[j→ i]* is a transfer function from *j* to *i*. The clique of *i* is the chosen neighborhood radius of *i*. For convenience, the radius is represented as number of hops.

$$T[j \to i] = \prod_{k=List(j,i)}^{k=i} \left(\frac{S_{k+1}}{\sum_{l=0}^{cliqueof(k)} S_l} \right) * \frac{1}{Dist(k, k+1)} \ , \qquad \textbf{(4.4)}$$

where S_i is the inverse of the shear modulus of the i^{th} node if it is a mass node and is the shear modulus if it is a spring node. *Dist(k,k+1)* is a function that represents the distance between the k^{th} and $k+1^{th}$ nodes. The minimum value of *Dist(k,k+1)* is set to be 1. *List(j,i)* is the list of nodes along the path from *j* to *i*. The equation (4.3) is absolute

convergent since the transfer function between any two nodes is always less than 1. The transfer for applied force among nodes is implemented iteratively as follows.

4.4 Iterative Solutions for Displacement Computation

We introduce two sets of accumulators for each node, which are named Shot and UnShot, respectively. While the former provides the final value of the position for a node, the latter indicates a number which needs to be distributed to its neighbors if it is greater than 0. A schematic representation of the applied force and accumulators are shown in Fig 4 and 5, respectively. During a sequence of iterations, a node *i* of maximum UnShot is chosen and is compensated using equations 4.5-4.7. It can be seen that as the UnShot accumulator reaches zero for all the nodes, the steady state *F[i]* of mass node *i* in the model will be given by the *Shot[i]* accumulator. The *F[j]* of spring node *j* is set to be the average of its two mass nodes. Thus we present an iterative algorithm that can compute the steady state position of each of the model nodes for a given applied force. The time variant accumulators are mathematically represented as follows

$$UnShot^{t}[j] = UnShot^{t-1}[j] + UnShot^{tt-1}[i] \times T[i \rightarrow j] . \quad \textbf{(4.5)}$$

$$Shot^{t}[i] = Shot^{t-1}[i] + UnShot^{t-1}[i] \times T[i \rightarrow i] . \quad \textbf{(4.6)}$$

$$UnShot^{t-1}[i] = 0 . \quad \textbf{(4.7)}$$

The above equations are repeated in the same order until the UnShot accumulator of all the nodes becomes 0.

5 Algorithm Results and Implementation Details

In this section we first discuss the accuracy and the convergence obtained using the proposed method with the physically-based simulation.[21, 29]. Finally we discuss the implementation of lung deformations. A regular mesh is considered for analyzing the deformation. A bending force (push at the center of the mesh) is applied on each node of the mesh and the subsequent deformation using the proposed method and Witkin's method [29] with Euler's integration is shown in Fig 6. The nodes are numbered in a row wise fashion. The difference is very minimal. The convergence in each of these methods for the same setup is as shown in Fig 7. The number of steps taken signifies the computational time required. It can be observed that the proposed method has a faster convergence than [29].

The convergence of the proposed method is now analyzed by comparing it with the pre-computation method suggested by [21], for a node in the above setup as shown in Fig 8. It can be seen that the proposed method converges faster than the exponential convergence. The run-time analysis of the proposed method is as shown in TABLE 5.1.

The deformation of a 3D lung model is implemented as follows. Fig 9a shows the initial shape of high-resolution lung models obtained from the visible human data set. The deformation is done by considering the lung physiology as explained in Section 3.0. The shear modulus assigned for each node is constrained by the regional alveoli expansion and the thoracic-cage movement whose detailed discussion is beyond the scope of this paper. [26, 27, 30] The accuracy of the shear modulus needs to be relative over a bounded region since the transfer functions consider their local average. The force applied on each node is based on the pressure applied and is set to be the same on each node. The displacement of a surface node is computed for a unit increase in the surface area of lungs for an increase in volume[25], using equation 4.5-4.7. The computation of hysteresis during breathing is out of the scope of this paper and is addressed separately. [31] The displacement of the nodes for further increase in volume is represented as a direct multiple of the displacement computed for a unit increase in the surface area. The deformed shape caused by inflation is shown in Fig 9b. The computational analysis is explained in TABLE 5.1. The run-time deformation is O(n) where n is the number of mass nodes.

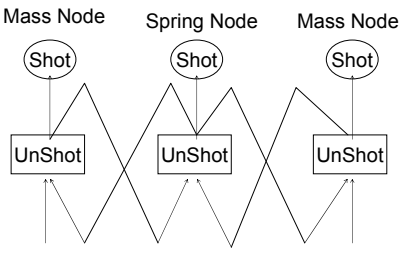

(Fig.5)

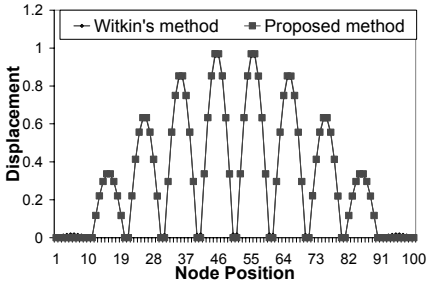

(Fig,6)

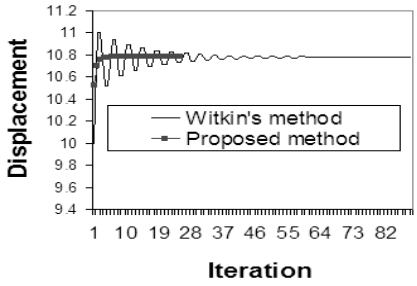

(Fig.7)

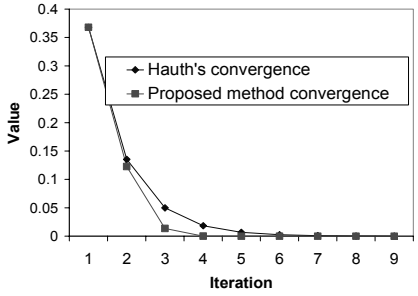

(Fig. 8)

Fig.5. Schematic representation of the use of accumulators for an iterative solution. **Fig.6.** A graph showing the deformation of a mesh grid in the direction of the applied force. **Fig.7.** A graph showing the convergence using the physically-based approach and the proposed approach. **Fig 8.** A graph showing the convergence of the iterative approach for an isotropic deformation of a node in a mesh grid. The proposed approach shows better convergence.

6 Conclusion

We were successfully able to pre-compute steady elastic deformations and we were able to deform a high-resolution lung model. The deformation being independent of the absolute assignment of initial shear modulus of each node facilitates easier creation of physically-based deformation. The faster convergence also provides real-time deformations which are highly suitable for AR environments. In the near future we will implement elastic deformations in Graphics Programming Unit hardware, to speed up the rendering process.

Acknowledgements

We wish to thank our sponsors the US Army STRICOM for their invaluable support for this research. We also thank Dr. Sumanta N. Pattanaik for his guidance and comments.

Table 1. Computational analysis of the proposed method and implementation system information.

Pre-computation Analysis				Implementation system information	
Clique Size M	Addition	Multiplications		CPU	Athlon 2800
M=1	O(N)	O(N)		GPU	GeForce4 Ti 4200
M>1	O(N)	O(N*M)		Shaders	NVIDIA CG 1.1
				Op. System	Linux Redhat 8.0

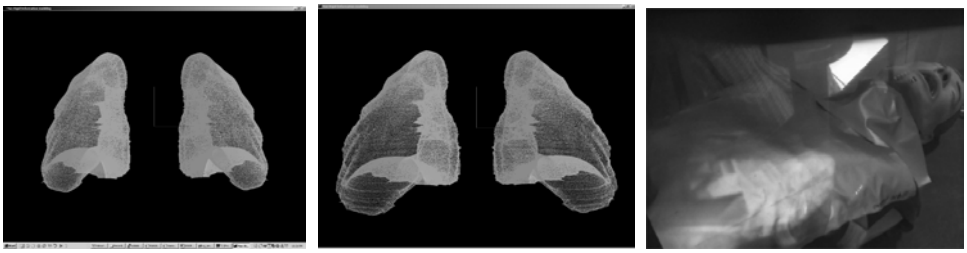

(Fig.9a) Initial Shape **(Fig.9b)** Deformed Shape **(Fig.9c)** Augmented View

Fig.9a-9c. The deformation of high-resolution lung models obtained from the visible human dataset, using the proposed approach. **Fig.9a** Shows the lung at residual volume (i.e. before inhalation). **Fig.9b** Represents the deformed lungs after inhalation. **Fig.9c** shows a snapshot of the breathing lungs super-imposed over the Human Patient Simulator and viewed in an AR Environment.

References

1. Satava, R.: Medical Virtual Reality:The current status of the future. Proceedings of 4th conference . Medicine Meets Virtual Reality. 1 (1996) 100-106.
2. DeCarlo, D., Kaye, J.M., Metaxas, D., Clarke, J.R., Webber, B., and Badler, N.I.: Integrating anatomy and physiology for behavior modeling. in Medical Meets Virtual Reality 3. San Diego (1995).

3. Terzopolous, D., Platt, J., Barr, A., and Fleisch, K.: Elastically Deformable Models. ACM Siggraph 1987. 21 (4) (1987) 205-214.
4. Ackerman, M.J.: The visible human project. Journal of Biocommunication. 18 (14) (1991).
5. Argotti, Y., Davis, L., Outters, V., and Rolland, J.P.: Dynamic Superimposition Of Synthetic Objects On Rigid And Simple-Deformable Objects. Computers and Graphics. 26 (6) (2002) 919--930.
6. Baraff, D. and Witkin, A.: Coping with friction for non-penetrating rigid body simulation. in Proceedings of Annual Conference of Computer Graphics and Interactive Techniques Siggraph 1991. ACM Press (1991).
7. Platt, S.M. and Badler, N.I.: Animating facial expressions. Proceedings of the 8th annual conference on computer graphics and interactive techniques, (1981) 245-252.
8. Desbrun, M., Schroder, P., and Barr, A.: Interactive animation of structured deformable objects. Graphics Interface 99, (1999).
9. Bro-nielsen, M.: Finite Element Modeling in Medical VR. Journal of the IEEE. 86 (3) (1998) 490-503.
10. James, D.L. and Pai, G.K.: Multiresolution Green's Function Methods for interactive simulation of elastostatic models. ACM Transactions of Graphics. 22 (1) (2003) 47-82.
11. White.R.E: An Introduction to Finite Element Methods. Raleigh,NC: John Wiley and Sons (1991).
12. Barrett, R., Berry, M., Chan, T.F., Demmel, J., Donato, J., Dongarra, J., Eijkhout, V., Pozo, R., Romine, C., and Van der Vorst, H.: Templates for the Solution of Linear Systems: Building Blocks for Iterative Methods, 2nd Edition. Philadelphia,PA: SIAM (1994).
13. Cotin, S. and Delingette, H.: Real-time Elastic Deformations of Soft Tissues for Surgery Simulation. IEEE transactions on Visualization and Computer Graphics. 5 (1) (1999) 62-71.
14. Zhuang, C.: Real-Time Simulation of Physically Realistic Global Deformations, in Computer Science Department. 1999, University of California,Berkeley Berkeley, CA.
15. Fung, Y.C.: Biomechanics: Mechanics properties of living tissues. New York: Spring (1993).
16. Green.A.E and Zerna.W: Theoretical Elasticity. Oxford: Clarendon Press (1968).
17. Delingette, H.: Towards realistic soft tissue modeling in medical simulation. Proceedings of IEEE: Special Issue on Surgery Simulation, (1998) 512-523.
18. Picinbono, G., Delingette, H., and Ayache, N.: Non-linear and anisotropic elastic soft tissue models for medical simulation. in ICRA. (2001).
19. Balanuik, R.: Soft-tissue simulation using LEM-Long Elements Method. Medicine Meets Virtual Reality, (2002) 38-44.
20. Balanuik, R. and Salisbury, K.: Soft-tissue simulation using the radial element methods. International Symposium on Surgery Simulation and Soft Tissue Modeling. 1 (2003) 48-58.
21. Hauth, M., Gross, J., Straber, W., and Buess, G.F.: Soft-tissue simulation based on measured data. Medical Image Computing and Computer Aided Intervention, (2003) 262-270.
22. Barber, J.R.: Elasticity. Solid Mechanics and its applications, ed. G.M.L. gladwell. Waterloo,Canada: Kluwer Academic publisher (1992).
23. Mead, J.: Measurement of Inertia of the Lungs at Increased Ambient Pressure. Journal of Applied Physiology. 2 (1) (1956) 208-212.

24. Ligas, J.R. and Primiano, F.P.J., *Respiratory mechanics*, in *Encyclopedia of Medical Instrumentation*, J.G. Webster, Editor John Wiley& Sons: New York (1988). 2550-2573.
25. Promayon, E., Baconnier, P., and Puech, C.: Physically-based model for simulating the human trunk respiration movements. Proceedings of International Joint Conference in CVRMED and MRCAS. 1205 (1997) 121-129.
26. Kaye, J.M., Primiano, F.P.J., and Metaxas, D.N.: A Three-dimensional virtual environment for modeling mechanical cardiopulmonary interactions. Medical Image Analysis. 2 (2) (1998) 169-195.
27. Segars, W.P., Lalush, D.S., and Tsui, B.M.W.: Modeling Respiratory mechanics in the MCAT and the spline-based MCAT systems. IEEE Transactions on Nuclear Science. 48 (1) (2001) 89-97.
28. Jones, E.R. and Childers, R.L.: Contemporary College Physics. McGraw-Hill Science/Engineering/Math 3rd Bk&Cdr Edition (2001).
29. Witkin, A., Baraff, D., and Kass: An Introduction to physics-based Modeling. 1997, Robotics Institute,Carnegie Mellon University. p. C1-C12.
30. Staub, N.C.: Basic Respiratory Physiology. New York: Churchill Livingstone (1991).
31. Santhanam, A., Fidopiastis, C., and Rolland, J.P.: An adaptive driver and real-time deformation algorithm for visualization of high-density lung models. in MMVR. Newport, CA (2004).